Program Digest, 2019 IEEE International Ultrasonics Symposium (IUS)
Glasgow, Scotland, October 6-9, 2019

Wavelet Regularized Born Inversion

Thomas G. J. Bouchan
Department of Imaging Physics
Faculty of Applied Sciences
Delft University of Technology
Delft, the Netherlands
Email: T.G.J.Bouchan@student.tudelft.nl

Ulas Taskin
Department of Imaging Physics
Faculty of Applied Sciences
Delft University of Technology
Delft, the Netherlands
Email: U.Taskin-2@tudelft.nl

Koen W. A. van Dongen
Department of Imaging Physics
Faculty of Applied Sciences
Delft University of Technology
Delft, the Netherlands
Email: K.W.A.vanDongen@tudelft.nl

***Abstract*—Breast ultrasound is gaining interest as an alternative to mammography. To improve its diagnostic value, full waveform inversion methods are developed. These methods aim for reconstructing speed of sound maps of the breast. When the inversion is performed in the frequency domain, computation time is reduced by limiting the number of frequency components at the cost of retrieving noisy images. To compensate for the lack of frequency information and to reduce the noise in the reconstruction, we propose two solutions. First, we select the frequency components randomly out of the entire available bandwidth for each source-receiver combination separately. Next, a regularization method is applied that takes advantage of the sparseness of the reconstructed contrast in the wavelet domain.**

***Index Terms*—wavelet regularization, Born inversion, breast ultrasound**

I. Introduction

Breast cancer is the most frequently diagnosed cancer among women. Detecting it at an early stage enables to significantly reduce the mortality rate [1]. Currently, mammography is the gold standard for screening. Unfortunately, it has some disadvantages, among which the difficulty to scan women with dense breasts. Ultrasound is a promising alternative enabling safe and fast diagnosis [2]. To ease the differention between malignant and benign tissues, waveform inversion methods have become of interest. With these methods speed of sound profiles of the breast are reconstructed [3].

When applying waveform inversion in the frequency domain, special attention is given to the selection of frequency components. It is common practice to select only a limited number of frequency components from the available bandwidth to reduce computation time [4], [5]. Another common practice is reffered to as frequency-hopping [6], which may be useful to avoid local minima.

To improve on convergence, regularization is employed when solving the inverse problem. The most common regularization techniques are related to the total variation [7] in and sparsity [8] of the reconstruction. Regularization is an important tool to stabilize the inversion.

In this work, regularized frequency domain Born inversion is investigated [9], [10]. To improve its convergence, the frequencies used for the inversion are chosen randomly over the available bandwidth for each source receiver combination, at the expense of additional noise in the reconstruction. To regularize the inverse problem and to reduce the amount of noise in the reconstruction, the sparsity constraint for the reconstruction in the wavelet domain is utilized. To test and validate Born inversion in combination with sparsity based regularization, a study has been performed using synthetic and real data.

II. Theory

The acoustic pressure field $p(\mathbf{x},\omega)$, where $\mathbf{x}$ denotes a position in the two-dimensional spatial domain $\mathbb{D}$ and ω is the angular frequency, can be decomposed into an incident field $p^{inc}(\mathbf{x},\omega)$ that is generated by the source and propagates in the homogeneous embedding, and a scattered field $p^{sct}(\mathbf{x},\omega)$ that equals

$$p^{sct}(\mathbf{x},\omega) = \omega^2 \int_{\mathbf{x}'\in\mathbb{D}} G(\mathbf{x}-\mathbf{x}',\omega)\chi(\mathbf{x}')p(\mathbf{x}',\omega)dV, \quad (1)$$

where $G(\mathbf{x}-\mathbf{x}',\omega)$ is the Green's function and $\chi(\mathbf{x}')$ is the contrast function given by

$$\chi(\mathbf{x}') = \frac{1}{c^2(\mathbf{x}')} - \frac{1}{c_0^2}, \quad (2)$$

where $c(\mathbf{x}')$ and c_0 are the speed of sound of the actual medium and of the homogeneous embedding respectively. Under the weak scattering approximation, the pressure field inside integral equation (1) can be replaced by the incident field, hence

$$p^{sct}(\mathbf{x},\omega) = \omega^2 \int_{\mathbf{x}'\in\mathbb{D}} G(\mathbf{x}'-\mathbf{x}',\omega)\chi(\mathbf{x}')p^{inc}(\mathbf{x}',\omega)dV. \quad (3)$$

This linearisation is known as the Born approximation. The unknown contrast function $\chi(\mathbf{x}')$ can be found by solving the minimization problem

$$\min_\chi \left\|\mathbf{d} - \mathrm{M}[\chi]\right\|^2, \quad (4)$$

where $\mathbf{d}$ is the measured scattered field and M is an operator representing integral formulation (3). To find the contrast function $\chi(\mathbf{x}')$, (4) is minimized using an iterative optimization method [9].

A. Frequency Selection

The minimization problem in (4) can be solved for different frequencies independently. In this work, we randomly select a unique set of frequencies for each source-receiver combination. By doing this, the computation time is reduced and

information from the entire available bandwidth is included in the reconstruction. However, limiting the total amount of data used for the reconstruction leads to an increase of the amount of noise in the reconstruction.

B. Wavelet Regularization

Wavelet regularization is used to filter the noise introduced by the random frequency selection. This noise has no spatial correlation and is represented by many coefficients with low intensity in the wavelet domain. At the same time, the image is often structured and may well be represented with only a few coefficients with a high amplitude in the wavelet domain. By applying a hard threshold in the wavelet domain, it is possible to filter out the noise. With the thresholding constraint, the minimization problem of interest becomes

$$\min_{\chi} \|\mathbf{d} - \mathrm{M}[\chi]\|^2 \quad s.t. \quad \|\psi[\chi]\|_0 < \alpha, \tag{5}$$

where ψ is the wavelet transform and α is the threshold value.

III. Results

A. Configuration

To acquire real data, four Philips P4-1 probes connected to a Verasonics Vantage 256 device are used. Each probe contains a linear array of 96 elements and is fixed in a holder during the measurement. The water tank has dimensions of $45\ \mathrm{mm} \times 45\ \mathrm{mm}$ and contains an agar based phantom [11]. The phantom has dimensions of $26\ \mathrm{mm} \times 29\ \mathrm{mm}$ and includes holes with diameters of $2\ \mathrm{mm}, 3\ \mathrm{mm}$ and $4\ \mathrm{mm}$, see Fig. 1.

First, an empty measurement, where the tank is only filled with water, is done to calibrate the system. From this empty measurement the incident field and the excitation pulse is retrieved. The excitation pulse has a center frequency of $1.5\ \mathrm{MHz}$. The measured wavelet and its spectrum are shown in Fig. 2. Next, a measurement with the phantom placed in the tank is done. The scattered field is obtained by subtracting the empty measurement from the phantom measurement.

A synthetic data set is generated by using a forward modelling method based on a frequency domain integral equation formulation [12]. The synthetic setup is designed to mimic the real measurement setup. The synthetic data is useful to evaluate the reconstruction method as it represents the ideal noise-free data for which the ground truth is known.

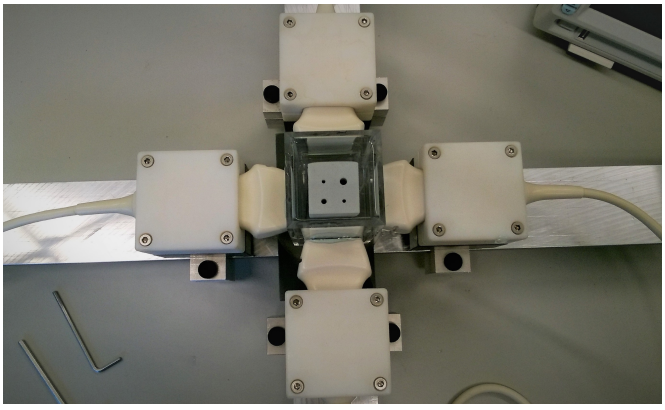

Fig. 1. Measurement setup.

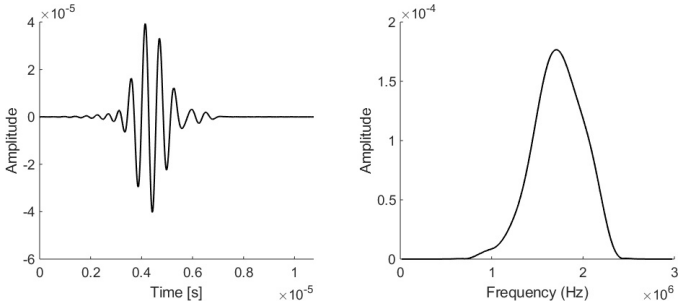

Fig. 2. Source excitation profile in time (left) and frequency (right) domain.

B. Randomizing

Within a predefined bandwidth, the same number of frequency components is randomly picked for each source-receiver combination. In the end, all frequencies from the available bandwidth are used in the same proportion. This is different from the commonly applied selection method, where the same frequency components are selected for all source-

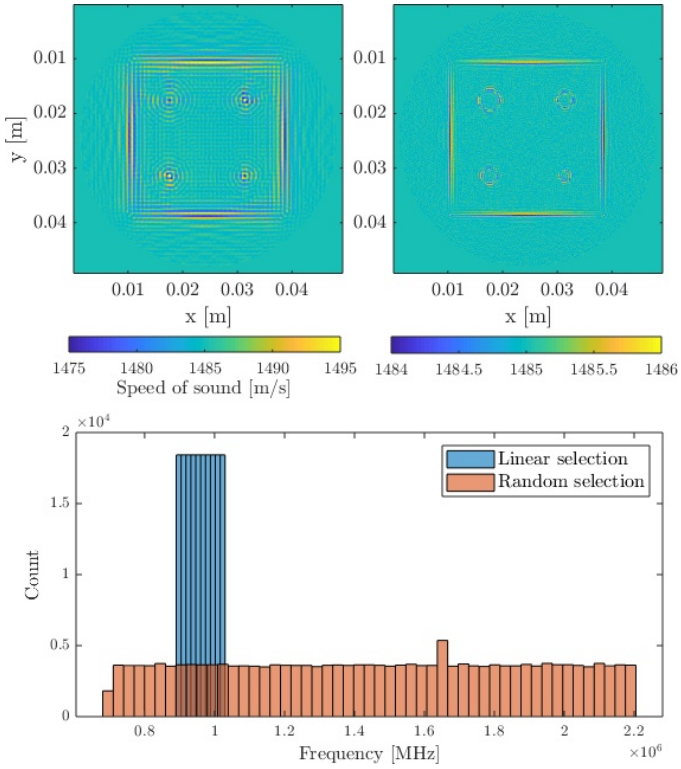

Fig. 3. Difference between linear and random selection of the frequencies. For both reconstructions only 10 frequency components from the available synthetic data are used, with synthetic data and only reflection signals. (Left) the ten frequency components are selected out of the same narrow band (0.9 - 1.05 MHz) for all source-receiver combination. (Right) the ten frequency components are selected randomly for each source-receiver combination out of the available bandwidth (0.7 - 2.2 MHz). (Bottom) histogram of frequency selection for both approaches.

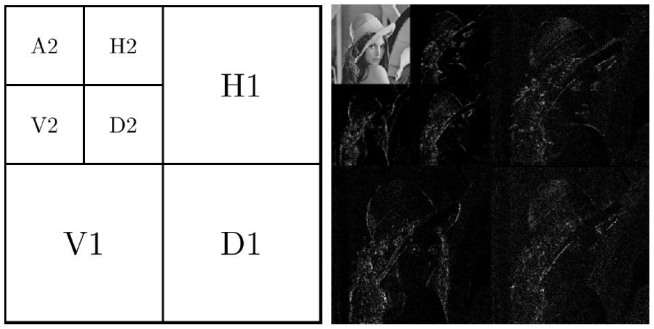

Fig. 4. Structure of the wavelet transform (left) and wavelet transform of Lena at level 2 using Daubechies 4 wavelet (right).

receiver combinations. Unfortunately, the latter technique does not allow for a wide coverage of the available bandwidth leading to a reconstruction of lower quality. Fig. 3 shows the difference in the reconstruction for those two techniques. Although the amplitudes of both images are not the same, the reconstruction with the random frequency selection has a better quality, it has sharper edges and shows less ringing effect and therefore leads to a better reconstruction of the holes. Fig. 3 also shows a histogram of the selected frequencies for the two methods.

C. Wavelet Regularization

A wavelet transform example is presented in Fig. 4. Here a two-level wavelet transform is performed on the well known Lena image using the commonly used Daubechies 4 wavelet. The first level gives four images of half the size of the initial image, which are the approximation (A1), horizontal (H1), vertical (V1) and diagonal (D1) details. To achieve a higher level decomposition the same scheme is applied on A1, to give A2, H2, V2, and D2. Fig. 4 presents the layout of those details. As can be seen the discrete wavelet transform is a one-to-one transformation, which means that the number of elements is conserved throughout the transformation. A majority of the coefficients have low amplitudes. Consequently, the information contained in the original image in the Cartesian domain is represented by only a few dominating coefficients in the wavelet domain. This is important for the use of this basis as a regularization tool.

D. Born Inversion Results

Born inversion with and without wavelet regularization are tested on synthetic and real data and compared with each other. The results are presented for reflections and transmissions measurements separately. A reflection image is produced by using only the data received by the probe containing the source. A transmission image is created from data received by the probe facing the source. All images are the result of Born inversion for ten frequencies randomly picked out of the bandwidth 0.7 - 2.2 MHz, and 16 iterations.

Results obtained with Born inversion with the synthetic data-set are presented in Fig. 5. The color scale is the same for all images. The regularization method does not change

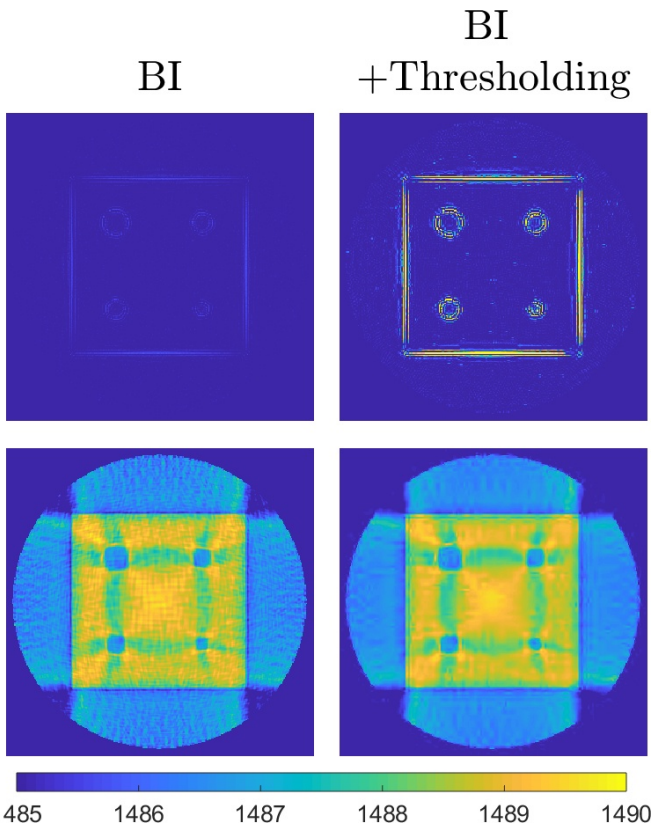

Fig. 5. Born inversion results for synthetic data-set. The first row shows the reconstruction obtained with reflection measurement. The second row shows the reconstruction obtained with transmission measurement.

the shape of the phantom but it does change the contrast and therefore the amplitude of the reflections. This phenomena does not appear in the reconstruction using transmission data only, where it would lead to errors in the speed of sound reconstruction. The thresholding method clearly denoises the image without affecting the shape of the phantom. Only the highest 2% of the coefficients have been used. This thresholding is performed from the 7th iteration onwards. In this way a good estimation of the reconstruction is obtained before applying a regularization which may change the shape of the contrast.

The reconstructions for measurement data are presented in Fig. 6. The colorbars are different for the two reconstructions to enhance the main characteristic of each reconstruction. With Born inversion without regularization, the contrast of the boundary of the holes is low and it is hard to distinguish them. With the regularized Born inversion method the holes become clearly visible. After thresholding, the noise is reduced with the boundaries preserved.

Fig. 7 shows the result of Born inversion with a varying proportion of coefficients being retained. The performance of the denoising process is optimal when the noise is reduced while the structure of the object remains unchanged.

IV. Conclusion

A new method to improve the performance of Born inversion is presented. It combines random frequency selection with

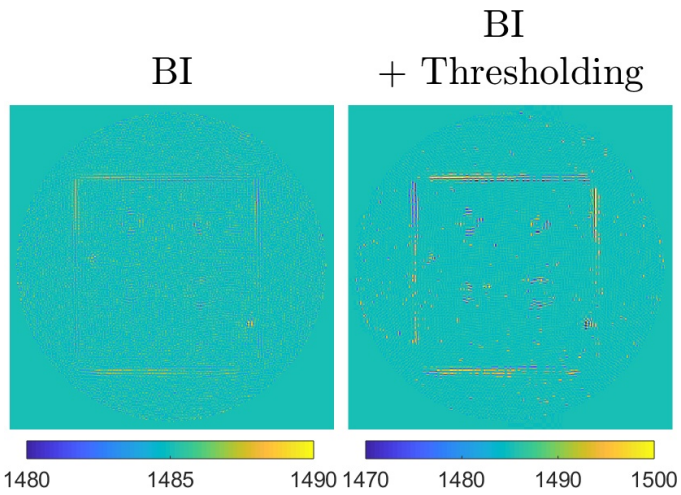

Fig. 6. Born inversion results for real measurement data. The reconstructions are obtained with reflection measurement.

hard thresholding of the contrast in the wavelet domain. The method has been successfully tested on both synthetic and real measurements and shown to reconstruct the object with a better accuracy than traditional Born inversion.

Although not tested, proposed methods are expected to work especially well in combination with interface contrast imaging which aims for reconstructing reflectivity images [13], [14].

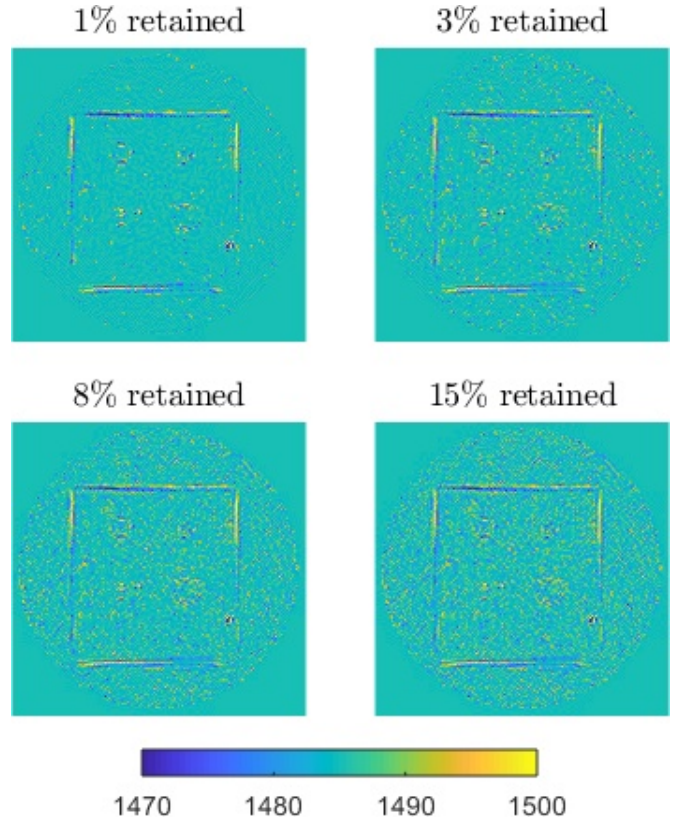

Fig. 7. Comparison of the results of Born inversion for different percentages of the coefficients retained.

References

[1] R. L. Siegel, K. D. Miller, and A. Jemal, "Cancer statistics, 2019," CA: a cancer journal for clinicians, vol. 69, no. 1, pp. 7–34, 2019.

[2] J. Geisel, M. Raghu, and R. Hooley, "The role of ultrasound in breast cancer screening: the case for and against ultrasound," In Seminars in Ultrasound, CT and MRI, vol. 39, no. 1, pp. 25–34, 2018

[3] N. Ozmen, R. Dapp, M. Zapf, H. Gemmeke, N. V. Ruiter, and K. W. A. van Dongen "Comparing different ultrasound imaging methods for breast cancer detection," IEEE Trans. Ultrason. Ferroelectr., Freq. Control, vol. 62, no. 4, pp. 637–646, 2015.

[4] L. Sirgue, and R. G. Pratt, "Efficient waveform inversion and imaging: A strategy for selecting temporal frequencies," Geophysics, vol. 69, no. 1, pp. 231–248, 2004.

[5] W. A. Mulder, and R. E. Plessix, "How to choose a subset of frequencies in frequency-domain finite-difference migration," Geophysical Journal International, vol. 158, no. 3, pp. 801–812, 2004.

[6] W. C. Chew, and J. H. Lin, "A frequency-hopping approach for microwave imaging of large inhomogeneous bodies," IEEE Microwave and Guided Wave Letters, vol. 5, no. 12, pp. 439–441, 1995.

[7] A. B. Ramirez, and K. W. A. van Dongen, "Sparsity constrained contrast source inversion," JASA, vol. 40, no. 3, pp. 1749–1757, 2016.

[8] A. Abubakar, and P. M. van den Berg, "Total variation as a multiplicative constraint for solving inverse problems," IEEE Transaction on Image Processing, vol. 10, no. 9, pp. 1384–1392, 2001.

[9] A. Abubakar, P. M. van den Berg, and S. Y. Semenov "A robust iterative method for Born inversion," IEEE TGRS, vol. 42, no. 2, pp. 342–354, 2004.

[10] A. B. Ramirez, and K. W. A. van Dongen "Sparsity constrained Born inversion for breast cancer detection," IEEE International Ultrasonics Symposium (IUS), 2015.

[11] R. M. Souza, T. Q. Santos, D. P. Oliveira, R. M. Souza, A. V. Alvarenga, and R. P. B. Costa-Felix "Standard operating procedure to prepare agar phantoms," In Journal of Physics: Conference Series, 2016.

[12] U. Taskin, N. Ozmen, H. Gemmeke, and K. W. A. van Dongen "Modeling breast ultrasound; on the applicability of commonly made approximations," Archives of Acoustics, vol. 43, no. 2, pp. 425–435. 2018.

[13] J. van der Neut, J. T. Fokkema, P. M. van den Berg, M. Zapf, N. V. Ruiter, U. Taskin, and K. W. A. van Dongen "Ultrasonic synthetic-aperture interface imaging," IEEE Trans. Ultrason. Ferroelectr., Freq. Control, vol. 66, no. 5, pp. 888–897. 2019.

[14] J. van der Neut, P. M. van den Berg, J. T. Fokkema, and K. W. A. van Dongen "Acoustic interface contrast imaging," Inverse Problems, vol. 34, no. 11, 2018.